Published in final edited form as:
Bioconjug Chem. 2011 March 16; 22(3): 455–465. doi:10.1021/bc100483k.

^{99m}Tc-Bisphosphonate-Iron Oxide Nanoparticle Conjugates for Dual-Modality Biomedical Imaging

Rafael Torres Martin de Rosales[*], **Richard Tavaré**, **Arnaud Glaria**, **Gopal Varma**, **Andrea Protti**, and **Philip J. Blower**
King's College London, Division of Imaging Sciences & Biomedical Engineering, 4th Floor Lambeth Wing, St. Thomas' Hospital, SE1 7EH, London, United Kingdom (U. K.)

Abstract

The combination of radionuclide-based imaging modalities such as single photon emission computed tomography (SPECT) and positron emission tomography (PET) with magnetic resonance imaging (MRI) is likely to become the next generation of clinical scanners. Hence, there is a growing interest in the development of SPECT- and PET-MRI agents. To this end, we report a new class of dual-modality imaging agents based on the conjugation of radiolabeled bisphosphonate (BP) directly to the surface of superparamagnetic iron oxide (SPIO) nanoparticles. We demonstrate the high potential of the BP-iron oxide conjugation using ^{99m}Tc-dipicolylamine(DPA)-alendronate, a BP-SPECT agent, and Endorem/Feridex, a liver MRI contrast agent based on SPIO. The labeling of SPIOs with ^{99m}Tc-DPA-alendronate can be performed in one step at room temperature if the SPIO is not coated with an organic polymer. Heating is needed if the nanoparticles are coated, as long as the coating is weakly bound as in the case of dextran in Endorem. The size of the radiolabeled Endorem (^{99m}Tc-DPA-ale-Endorem) was characterized by TEM (5 nm, Fe_3O_4 core) and DLS (106 ± 60 nm, Fe_3O_4 core + dextran). EDX, Dittmer-Lester and radiolabeling studies demonstrate that the BP is bound to the nanoparticles and that it binds to the Fe_3O_4 cores of Endorem, and not its dextran coating. The bimodal imaging capabilities and excellent stability of these nanoparticles were confirmed using MRI and nanoSPECT-CT imaging, showing that ^{99m}Tc and Endorem co-localize in the liver and spleen *in vivo*, as expected for particles of the composition and size of ^{99m}Tc-DPA-ale-Endorem. To the best of our knowledge, this is the first example of radiolabeling SPIOs with BP conjugates and the first example of radiolabeling SPIO nanoparticles directly onto the surface of the iron oxide core, and not its coating. This work lays down the basis for a new generation of SPECT/PET-MR imaging agents in which the BP group could be used to attach functionality to provide targeting, stealth/stability and radionuclides to Fe_3O_4 nanoparticles using very simple methodology readily amenable to GMP.

Keywords

Bisphosphonates; Iron oxide nanoparticles; Dual-modality Imaging; Imaging Agents; Magnetic resonance imaging; Single photon emission computed tomography

rafael.torres@kcl.ac.uk.

Europe PMC Funders Author Manuscripts

Introduction

Medical imaging techniques allow us to look inside the human body and detect diseased tissue without the need of surgery (1). Two of the most common imaging techniques are single photon emission computed tomography (SPECT) and positron emission tomography (PET). These modalities rely on the properties of radionuclides. Other techniques like magnetic resonance imaging (MRI) use magnetic fields to detect water molecules in different tissue environments, sometimes aided by paramagnetic metal-based contrast agents.

Each of these imaging modalities has its own strengths and weaknesses. For example, radionuclide-based techniques (SPECT/PET) are extremely sensitive and therefore allow us to study processes at the molecular and cellular level *in vivo*. Their spatial resolution, however, is poor (≥1 cm for a clinical scanner). On the other hand, non-radionuclide based techniques such as computed tomography (CT) and MRI provide excellent spatial resolution (<0.1 cm), but require much larger amounts of contrast agent. It is the need to overcome their respective disadvantages that is driving the ongoing efforts to develop dual modality imaging instruments and agents so that the strengths of these techniques can be synergistically combined to provide accurate physiological and anatomical information. Some of these instruments are being used nowadays in the clinic (*e.g.* SPECT-CT and PET-CT) in which the SPECT or PET component provides molecular information on the physiology and the CT component provides anatomical information. The next generation of dual modality instruments being developed today is based in the combination of SPECT/PET and MRI (2–6). The use of MRI as a substitute for CT benefits from (*i*) no radiation dose to patients;[1] (*ii*) higher anatomical soft-tissue contrast (7–12); (*iii*) and the possibility of simultaneous acquisition of the two modalities (PET-MR), reducing the time spent by patients in the scanner and the assurance that the two modalities are being taken under the same physiological conditions and spatial positioning. Furthermore, clinically-effective MRI contrast agents based on paramagnetic metals are commonly used, opening up the attractive idea of using dual modality SPECT-CT or PET-MR imaging agents (13–17). Having a bimodal agent with a “single pharmacological behavior” means that the advantages of both imaging modalities, such as the high sensitivity of PET and the high resolution of MRI, can be combined into a single image with confidence that both images reflect the same biological process. At the same time, their individual disadvantages are minimized. The synergistic effect of dual-modality imaging agents and techniques should make quantification of the signal more accurate, allowing clinicians to diagnose, plan treatments and monitor their outcomes more precisely. For example, *in vivo* quantification of the biodistribution of SPIO-based contrast agents using MRI is often difficult to perform. This is mostly due to the strong susceptibility effect of superparamagnetic materials that results in significant signal loss in tissues where the material accumulates. Furthermore, *in vivo* micro-environment-dependent changes of the relaxometric properties of SPIOs as well as the complex methodology required complicate the process further. On the other hand, *in vivo* quantification of photons emitted by radionuclides using SPECT/PET instrumentation is an

[1]It has been estimated that the radiation dose of a full-body CT scan is equivalent to that of more than 500 X-ray scans and similar to what people at 2.4 kilometres away from the World War II atomic blasts received in Japan.

accurate and relatively fast process that, unlike MRI methods, is independent of the SPIO micro-environment *in vivo*. Hence, by adding a SPECT or PET component to SPIO agents, the higher sensitivity of these techniques allow easy and accurate quantification of their biodistribution, even with very low amounts of SPIO. Other potential clinical applications of dual-modality agents would be to use the radionuclide component to locate areas of interest prior to detailed anatomical analysis by MRI or to use both the SPECT/ PET and MR signals from the dual-modality contrast agent as reference points for fusing the images from both modalities together.

Despite the high potential of these agents for finding applications in medical imaging, reports of SPECT- or PET-MR agents are still rare (13–17). These reports are based on radiolabeling superparamagnetic iron oxide (SPIO) nanoparticles with SPECT or PET isotopes (18–28). SPIOs are one of the most successful nanotechnological tools available today in the clinical field, and are extensively used as MRI contrast agents (29–32). Another potential use is as therapeutic agents, as SPIOs generate enough heat under alternating magnetic fields to kill surrounding cells by hyperthermia (33, 34). In order to radiolabel SPIOs, their surface must be functionalized with radionuclide-binding molecules, such as chelators. To date, this has been done by standard conjugation chemical reactions with the polymeric coatings that are needed to impart sufficient colloidal stability to the particles (19–28). The coatings, however, are normally only weakly-bound to the surface of the particle, which may result in decomposition over time and consequent loss of colloidal stability (35, 36). This problem, however, can be solved for certain coatings by cross-linking the polymer (37).

A recent and as yet unexplored approach to coat iron oxide NPs is the use of bisphosphonates (BPs, Figure 1). BPs are well known drugs in the osteoporosis and oncology fields due to the fact that they bind avidly to the surface of metabolically-active bone. However, it is less well known that BPs also bind very strongly to metallic surfaces. In fact, BPs have been used for more than a century to prevent the corrosion of iron-based metals like steel, implying their strong binding to the surface to inhibit oxidation (38). Recently BPs were “re-discovered” as strong binders of iron oxide surfaces (39–46). Remarkably, the binding is strong enough to allow the BP to stay bound to the metallic or metal oxide surface for at least a month at pH 7 (39). This is in contrast to other chemical groups such as monocarboxylates, monosulfonates and phosphates, commonly used as coating agents for iron oxides (39). Some polycarboxylates such as citrate, disulfonates, phosphonates, and particularly catechols form stable complexes with iron oxides and their ability to coat SPIOs has been demonstrated (47–50). It has been noted, however, that catechols may react through a redox mechanism with the surface of iron oxide nanoparticles in protic environments, leading to decomposition and precipitation of the nanoparticles (51).

There is a growing interest in developing non-polymeric, biocompatible methods to coat SPIOs for biomedical applications, and the use of BPs as “molecular anchors” may be a promising approach but has hardly been exploited to date. To the best of our knowledge, there are only two reports in the literature using such approach for diagnostic/therapeutic purposes, both from Motte *et al.* (44, 45). This group has recently shown that SPIO nanoparticles can be coated with BPs and that they can be further functionalized with a

fluorescent tag. The particles retained their magnetic properties and thus function as a dual-modality fluorescence-MRI contrast agent *in vitro*. Here, we show that the concept can be extended to making agents for *in vivo* SPECT-MR and hence, in principle, PET-MR imaging. We demonstrate it by conjugating Endorem, a clinically approved SPIO for liver MR imaging, with a radiolabeled BP tracer. The product retains its *in vivo* MRI contrast properties and biodistribution while gaining SPECT imaging properties from the BP tracer. The SPECT signal allows easy and accurate quantification using widely available instrumentation, providing a simple method for organ biodistribution studies of SPIO-based MRI agents using SPECT instrumentation. These experiments provide the basis for a new generation of PET/SPECT-MR dual-modality medical imaging agents in which the BP may be used as a stable anchor of signaling, targeting and stability/stealth molecules onto the metallic surface of iron oxide nanoparticles.

Experimental Procedures

Materials

Reagents and materials were obtained from commercial sources and used as received unless otherwise noted. Organic solvents were of HPLC grade. Dipicolylamine-alendronate (DPA-ale) and ^{99m}Tc-DPA-alendronate were synthesized as previously reported (52). Water (Type I, 18.2 MΩ·cm) was obtained from an ELGA Purelab Option-Q system. Endorem was obtained from Guerbet GmbH (France) and used as received. Human serum from human male AB plasma was obtained from Sigma-Aldrich. For TLC studies, silica gel 60 F254 glass plates (2.5 × 7 cm, Merck KGaA, Germany) were used whereas ITLC-SG plates (Pall Sciences, USA) were used for ITLC studies. Dittmer-Lester's TLC reagent for the detection of phosphorus was prepared following the original literature protocol (53). TLC and ITLC plates were scanned with a Mini-Scan TLC Scanner equipped with a FC3600 detector of γ photons (Lablogic, UK). Reverse phase (RP) HPLC analyses were carried out using an Agilent 1200 series HPLC system (Agilent, USA) equipped with a quadruple pump, a vacuum-degasser, a UV detector set at 254 nm and a γ detector as for TLC above. For RP studies, Zorbax Eclipse XDB-C18 columns (5 μm, 4.6 x 150 mm) were used (Agilent, USA). Radioactivity in samples was measured with a CRC-25R dose calibrator (Capintec, USA) or a 1282 CompuGamma gamma counter (LKB Wallac, Finland). $[^{99m}Tc(CO)_3(H_2O)_3]^+$ was synthesized using Isolink kits (Mallinckrodt Medical B.V., St. Louis, MO, USA) (52, 54). Radiolabelled nanoparticles were purified using Vivaspin 500 filters with a 10 kDa molecular weight cut-off (GE Healthcare, UK). The concentration of uncoated magnetite SPIO nanoparticles was calculated by freeze-drying a sample of the solution and weighing the residue. 13 mm Millex IC 0.22 μm hydrophilic PTFE filters (Millipore, USA) were used throughout this study. Na[$^{99m}TcO_4$] in physiological saline was obtained from a ^{99}Mo/^{99m}Tc generator at the Radiopharmacy at Guy's and St Thomas' Hospital NHS Trust, London, UK.

Synthesis of ^{99m}Tc-DPA-ale

The complex ^{99m}Tc-DPA-ale was synthesized and characterized as previously described (52). Briefly, 1 μg of DPA-ale in 100 μL of 50 mM carbonate buffer (pH = 9, [NaCl] = 0.15 M) was mixed with 500 μL of an aqueous solution of $[^{99m}Tc(CO)_3(H_2O)_3]^+$ (500-800 MBq)

in a screw-cap vial that was sealed and heated at 100 °C for 30 min. The vial was then cooled in an ice bath and analyzed for purity by radio-HPLC and radio-TLC (52). Radiochemical purity was >99%.

Synthesis of uncoated SPIO magnetite nanoparticles (SPIO)

The synthesis of monodisperse SPIO magnetite nanoparticles lacking coating molecules was performed following an established method by Stroeve *et al* (55). The nanoparticles were synthesized 24 h before use and kept in degassed water under an inert atmosphere until use. Prior to radiolabeling the nanoparticles were filtered through a 0.22 μm hydrophilic PTFE filter to remove any potential aggregates. TEM studies and visual inspection showed that the uncoated SPIO nanoparticles aggregate within a few days.

Synthesis of ^{99m}Tc-DPA-ale-Endorem

The pH of a 500 μL solution of ^{99m}Tc-DPA-ale (270 MBq) was lowered from 9 to 7 by adding approximately 20 μL of a 0.1 M HCl solution. Then, 20 μL of Endorem (224 μg Fe) were added and the vial sealed and incubated at room temperature or 100°C for various times (once labeling conditions were established a standard incubation of 15 min at 100 °C was adopted to produce labeled particles for further study). The vial was then cooled in an ice bath and the contents transferred to a Vivaspin 500 filter with a 10 kDa molecular weight cut-off membrane that had been previously washed with 3 × 500 μL of H_2O. The filter was centrifuged at 12,000 g for 3 min, separating approximately 50 μL of retentate that contained the radiolabeled nanoparticles from 450 μL of filtrate that contained most of the unbound ^{99m}Tc-DPA-ale. To the retentate was added 100 μL of saline and the mixture sonicated for 1 min and centrifuged as before. This process was repeated 5 times until no more unbound ^{99m}Tc-DPA-ale was detected in the filtrates. The total radioactivity in the filtrates and retentates was measured to determine the radiolabeling yield (%). The retentate solution containing ^{99m}Tc-DPA-ale-Endorem was then made up to 100 μL by adding saline, mixed, removed from the Vivaspin filter and filter-sterilized using a 0.22 μm hydrophilic PTFE filter (13 mm-diameter). This step was necessary for the *in vivo* studies in order to avoid potential dust particles and bacteria that may compromise the wellbeing of the animals after *i.v.* injection of the agent. Less than 5% total radioactivity was retained in both filters (10 kDa size-exclusion and sterilizing), meaning that, if any, less than 5% of the nanoparticles were present as aggregates bigger than 220 nm after the labeling process.

Synthesis of ^{99m}Tc-DPA-ale-SPIO

The radiolabeling of uncoated SPIO nanoparticles synthesized as described above was performed as above for Endorem but at room temperature and using 150 μg of uncoated SPIO nanoparticles. Visual inspection showed that radiolabeled SPIO nanoparticles were colloidally unstable and precipitate in saline solution within 2 h.

Synthesis of DPA-ale-Endorem for characterization

The pH of a solution containing 1 μg of DPA-ale in 100 μL of 50 mM carbonate buffer (pH = 9, [NaCl] = 0.15 M) was lowered to 7 by adding approximately 20 μL of a 0.1 M HCl solution. 20 μL of Endorem (224 μg Fe) were then added and the vial sealed and heated at

100 °C for 15 or 30 min. The vial was then cooled in an ice bath and the contents transferred to a Vivaspin 500 filter with a 10 kDa molecular weight cut-off membrane that had been previously washed with 3 × 500 μL of H_2O. The labeled nanoparticles were purified as above for ^{99m}Tc-DPA-ale-Endorem. Washing of the retentate was stopped when no more phosphorus was detected in the filtrate by spotting a sample of the filtrate in a silica TLC plate and staining using Dittmer-Lester's reagent. The labeled nanoparticles where then made up to 100 μL by adding saline, mixed and removed from the Vivaspin filter. In order to resemble the material used for the *in vivo* studies and to remove dust particles that interfered with the DLS studies, the colloidal solution was filtered using a 0.22 μm hydrophilic PTFE filter (13 mm diameter). The filtering procedure removes less than 5% of the labeled nanoparticles (See synthesis of ^{99m}Tc-DPA-ale-Endorem). The binding of the bisphosphonate to Endorem was confirmed by EDX studies and Dittmer-Lester's test.

In vitro stability studies in PBS and human serum

To assess the *in vitro* stability of the BP-Fe_3O_4 bond in ^{99m}Tc-DPA-ale-Endorem and ^{99m}Tc-DPA-ale-SPIO (as a suspension of the precipitate in a non-colloidal solution), triplicate experiments with 10 μL of a solution of these compounds (~15 MBq) were incubated in PBS (500 μL) and human serum (500 μL) in a 5% CO_2/95% air atmosphere at 37 °C and constant shaking for 48 h. Aliquots of 250 μL were taken at 1, 24 and 48 h after mixing and these were centrifuged at 17,000 g for 15 min. The radioactivity of the pellets and supernatants of these aliquots were measured to give the percentage of radioactivity bound to the nanoparticles. After the measurement, the supernatant and pellet were mixed with the remaining sample and returned to the incubator.

Attenuated total reflection infrared (ATR-IR) spectroscopy

IR studies of lyophilized DPA-ale-Endorem and Endorem were performed in a Perkin-Elmer Spectrum 100 spectrometer equipped with a universal ATR sampling accessory.

Transmission electron microscopy (TEM) and energy dispersive X-ray (EDX) spectroscopy

TEM analyses were performed in a FEI Tecnai T20 instrument with a LaB_6 filament operating at 200 kV. The microscope was equipped with an energy-dispersive X-ray spectrometer (EDAX Genesis system), that allowed the detection of the elements present in each sample. The samples were prepared by evaporation of a drop of the aqueous colloidal suspensions onto a carbon-coated copper grid (Agar Scientific 200 mesh).

Dynamic Light Scattering (DLS)

DLS measurements were performed with a Beckman Coulter DelsaNano C instrument at 25°C.

In vitro MR and SPECT-CT imaging

Magnetic Resonance Imaging (MRI) scanner—MR imaging was performed on a wide-bore vertical 400 MHz (9.4 T) MR scanner (Bruker Avance III, Germany). The gradient coil had an inner diameter of 40 mm and gradient strength was 800 mT/m. A

quadrature transmit/receive coil with an internal diameter of 35 mm was used. Temperature was maintained at 37 °C using warm water running through the gradient coil.

SPECT-CT scanning—SPECT images were obtained with a nanoSPECT-CT preclinical animal scanner (Bioscan Inc., France) equipped with four heads, each with nine 1 mm pinhole collimators, in helical scanning mode in 20 projections over 15 min. The CT images were obtained with a 45 kVP X-ray source, 1000 ms exposure time in 180 projections over ~10 min. Images were reconstructed in a 256 × 256 matrix using the HiSPECT (Scivis GmbH) reconstruction software package, and fused using proprietary Bioscan InVivoScope (IVS) software. Quantification was performed by selecting the desired organs as regions of interest (ROI) using the quantification tool of the IVS software.

***T_2* relaxation measurement *in vitro*—**Samples of DPA-ale-Endorem and Endorem were prepared with Fe concentrations of 2.78, 1.39, and 0.69 mM by serial dilution, along with a control sample (0.00 mM Fe). For comparison a multiple echo spin-echo sequence was acquired with the following sequence: FOV = 40 × 40 mm^2; resolution = 0.156 × 0.156 mm^2; slice thickness = 1.5 mm; deltaTE/TR = 10/2000 ms and 16 echoes. Quantitative parameter maps of the transverse R_2 relaxation rate were produced using the image data acquired from multiple echo times (TEs). The signal, S(TE) at each pixel was fitted to a model for mono-exponential decay with TE: $S(TE) = S_0 \cdot \exp(-R_2 \cdot TE)$, where S_0 represents the signal intensity at TE = 0 ms and $R_2 = 1/T_2$. The average R_2 value within each sample was calculated using regions of interest in the parameter maps and plotted against the Fe concentration of each sample.

Phantom studies—Two samples of ^{99m}Tc-DPA-ale-Endorem (50 kBq, 100 μg Fe) were prepared in equal volumes and at equal concentrations in 1.5 mL microcentrifuge tubes. One sample was centrifuged to form a pellet. The two tubes were then taped together and carefully placed inside a 50 mL plastic centrifuge tube and water was added until the two sample tubes were covered. MR images were acquired in a plane allowing simultaneous imaging of both samples to demonstrate the effect of the iron-oxide based agent in solution and in pellet form. MR data were acquired with the following gradient-echo sequence: FA = 40°; FOV = 50 × 50 mm^2; resolution = 0.195 × 0.195 mm^2; slice thickness = 1.0 mm; and TE/TR = 10/350 ms. The sample tubes were then removed from the 50 mL centrifuge tube and transferred to the nanoSPECT-CT scanner and an image acquired as described above.

***In vivo* MR and SPECT-CT imaging—**The *in vivo* imaging procedure was carried out in accordance with British Home Office regulations governing animal experimentation and performed as follows. A healthy six-week-old female C57BL/6 mouse was anesthetized by subcutaneous injection of 200 μL of a mixture of 10% Dormitor (medetomidine) and 6.8% Vetalar (ketamine hydrochloride) in saline. After 15 min the mouse was placed in prone position on the MRI mouse bed and a pressure-transducer was placed under the abdomen for respiratory monitoring. Typical respiration rates were between 40 ± 10 min^{-1} (1500 ± 500 ms per respiratory cycle). Cine-FLASH was used to acquire temporally resolved dynamic short-axis MR images of the liver. The gradient echo technique maintains the steady-state during the entire scan. Spoiler gradients of 1 ms duration and 100 mT/m strength were

applied after each data acquisition readout to dephase the remaining transverse magnetization before the application of the next radio frequency (RF) excitation pulse. Cine-FLASH T_2*-weighted was performed without the use of triggering. Imaging parameters were as follows: repetition time (TR) = 300 ms; echo time (TE) = 2, 3, 4, 6, 8 ms; field of view (FOV) = 30 x 30 mm; matrix size = 128 ×128; slice thickness = 1 mm; flip angle = 30°; 3 averages, 5 slices, 1 frame. The acquisition time was 10 ± 0.5 minutes. Short axis and coronal views of the liver were acquired. The mouse was then injected a solution of ^{99m}Tc-DPA-ale-Endorem in saline (25 μL, 37 MBq, 56 μg Fe) intravenously (*i. v.*) via the tail vein and the same MRI scans were repeated 15 min post-injection. T_2* values in the liver were calculated by fitting the data to a model for mono-exponential decay using the same method as in the "T_2 relaxation measurement in vitro" section (*vide supra*), where T_2 was replaced by T_2*. At 45 min post-injection, the animal was imaged using the nanoSPECT/CT preclinical animal scanner as described above.

Biodistribution studies—Biodistribution studies were carried out in accordance with British Home Office regulations governing animal experimentation. Three mice were injected *i.v.* via the tail vein with 1 MBq (1.5 μg Fe) of ^{99m}Tc-DPA-ale-Endorem in 100 μL of physiological saline. After 1 hour, the mice were culled by cervical dislocation and the following organs were explanted; femur, kidneys, heart, stomach, spleen, intestines, liver, lung, muscle and a sample of blood. Each sample was weighed and counted with a gamma counter, together with standards prepared from a sample of the injected material. The percent of injected dose per gram of tissue was calculated for each tissue type.

Results and Discussion

Scheme 1 summarizes the procedure for radiolabeling SPIO nanoparticles using ^{99m}Tc-bisphosphonates. In a recent report we described the design, synthesis and characterization of a radiolabeled BP conjugate, ^{99m}Tc-DPA-ale (Scheme 1A), and demonstrated its bone-seeking capabilities (52). This compound is based on alendronate, a well-known and widely-used BP used to treat osteoporosis (56). One of the most attractive properties of ^{99m}Tc-DPA-ale is the high *in vivo* stability towards oxidation and ligand substitution of the ^{99m}Tc(I) metal centre provided by the tricarbonyl group. ^{99m}Tc-DPA-ale targets remodeling bone thanks to its BP group. The complex is highly stable *in vivo* and can be easily synthesized in water by treating the ligand (DPA-ale) with the complex *fac*-$[^{99m}Tc(CO)_3(H_2O)_3]^+$ at 100 °C. In this work we exploited the bisphosphonate group for its ability to bind to SPIO rather than for its bone-targeting properties. In order to establish that the radiolabeled BP was capable of binding SPIO nanoparticles, initial labeling experiments were performed by simply mixing ^{99m}Tc-DPA-ale with uncoated SPIO nanoparticles in water solution for 15 min at room temperature. This resulted in high radiolabeling yields (>95%) (Scheme 1B, top). Different pH conditions were tested (pH 5 to pH 7) and made no significant difference to the radiolabeling yields. Whether conjugated to ^{99m}Tc-DPA-ale or not, uncoated SPIO nanoparticles were colloidally unstable and precipitated within minutes due to the presence of physiological amounts of salt in the solution, preventing further studies. We then turned our attention to Endorem (Scheme 1B, bottom), a clinically-approved and colloidally stable MRI contrast agent that is taken up by cells of the reticuloendothelial system (RES) such as

the monocytes, macrophages and Kupffer cells found in the spleen and liver. Endorem, like other clinically-approved nanoparticle imaging agents approved for human use to date, is not a targeted nanoparticle agent and relies in its size and surface composition to reach its target. Endorem is composed of SPIO nanoparticles of magnetite enclosed in a biocompatible polymer (dextran) that imparts colloidal stability and surface properties to the system under physiological conditions. We first tried radiolabeling Endorem with ^{99m}Tc-DPA-ale by mixing solutions of the two compounds at room temperature for 15 min followed by separation of unbound ^{99m}Tc-DPA-ale from ^{99m}Tc-DPA-ale-Endorem by means of a centrifugal filter with a molecular weight cut-off of 10 kDa. Labeling at this temperature resulted in very low labeling yields (<10%). We attributed this result to the presence of dextran polymer associated with the surface of the nanoparticles. This coating, however, is relatively weakly-bound to the SPIO core of the nanoparticles (35, 36, 57). We thus hypothesized that increasing molecular motion by increasing the temperature should improve the access of the radiolabeled bisphosphonate to the surface of the iron oxide particles (Scheme 1B, bottom). Indeed, radiolabeling yields of >95% can be obtained by heating the reaction at 100 °C for 60 min., but these conditions cause substantial loss of colloidal stability and precipitation of a large fraction of the nanoparticles, presumably by extensive dissociation of the dextran-SPIO complex after prolonged high temperature (*vide infra*). This is not surprising as dextran is thought to be associated to the iron oxide nanoparticles by hydrogen bonding (57). After several trials, we established that performing the reaction for 15 min at 100 °C was sufficient to obtain radiolabeling yields of 55% (650 MBq/mg Fe) while maintaining the colloidal stability of the solution.[2] A non-radioactive analogue (DPA-ale-Endorem) was also synthesized for characterization purposes using the same procedure. DPA-ale-Endorem can be considered as a true mimic of ^{99m}Tc-DPA-ale-Endorem as both contain virtually the same amount of DPA-ale, which is several orders of magnitude higher than the amount of ^{99m}Tc-DPA-ale in the latter.

The composition and size of DPA-ale-Endorem and Endorem particles were studied using IR, TEM, EDX and DLS. The IR spectrum of lyophilized DPA-ale-Endorem demonstrates that the labeling and purification process had not resulted in the loss of the dextran coating. This is critical, as the dextran coating is necessary for stability. Thus, the spectra of both compounds are dominated by the vibrations of adsorbed dextran which obscure the iron oxide and bisphosphonate vibrational modes (Figure S1, supporting information) (57). Characteristic dextran vibrations were found at 3195 cm^{-1} (broad, O-H stretching), 2936 cm^{-1} and 1300-1450 cm^{-1} (C-H vibrations), 1020-1082 cm^{-1} (C-O vibrations) and ~880-930 (α-glucopyranose ring deformation modes) (57, 58). The presence of the bisphosphonate in DPA-ale-Endorem was demonstrated qualitatively by a simple spot test using Dittmer-Lester's reagent as well as by EDX (Figure 2D-E). Spotting a TLC silica plate with dilute samples of Endorem and DPA-ale-Endorem and staining with this reagent demonstrated the presence of the bisphosphonate by the appearance of a blue color in the latter, indicative of the presence of phosphorus in DPA-ale-Endorem, but not in Endorem (Figure 2A).

[2]This radiochemical yield allow us to calculate that the BP binds to 3% of the total surface area available at the 5 nm iron oxide nanoparticles (0.56×10^{15} nm^2). The calculation was made taking into account the amount of iron present in the reaction (4×10^{-6} moles), the amount of DPA-ale (2.33×10^{-9} moles), and making the assumption that each 5 nm nanoparticle (78 nm^2 surface area) contains 10×10^3 Fe atoms.

Elemental analysis using EDX is also in agreement with this observation, revealing the presence of phosphorus in DPA-ale-Endorem (Figure 2E). Despite the high affinity of BPs towards iron oxides, these techniques do not discriminate ^{99m}Tc-DPA-ale bound to the metallic surface of the nanoparticle from any associated with the dextran coating. To discount the latter possibility we prepared a concentrated solution of dextran (9 mM) and added a solution of ^{99m}Tc-DPA-ale (5 MBq), followed by 15 min heating at 100 °C. These conditions were chosen in order to mimic the radiolabeling conditions used and high concentration of the dextran coating around the Fe_3O_4 cores of Endorem. After cooling the mixture to room temperature, it was transferred to a 10 KDa centrifugal filter, centrifuged and the retentate washed several times with saline. ^{99m}Tc-DPA-ale quantitatively eluted from the filter, separating from the dextran solution. Increasing the reaction time had no effect in the result. When the same experiment was repeated in the presence of uncoated SPIOs (300 μg), 85% of ^{99m}Tc was retained in the filter and hence bound to the SPIO-dextran mixture. Furthermore, in agreement with the trend found with Endorem (*vide supra*), increasing the reaction time to 30 min resulted in almost quantitative binding to the SPIO-dextran mixture. Thus, these experiments strongly suggest that ^{99m}Tc-DPA-ale is not simply buried within the dextran coating in ^{99m}Tc-DPA-ale-Endorem but instead binds through its BP group to the surface of the metal core of Endorem, as shown in Scheme 1.

The size of DPA-ale-Endorem nanoparticles was investigated by TEM showing that the iron oxide core is morphologically indistinguishable from that of its precursor Endorem, with a mean particle size of 5 nm (TEM, Figure 2B-C, top). DLS studies, however, reveal that the average hydrodynamic size of DPA-ale-Endorem is 106 ± 60 nm, compared with 121 ± 67 nm for Endorem, suggesting that the labeling process slightly affects the hydrodynamic size of the nanoparticles (Figure 2B-C, bottom).[3] In order to determine the cause for the decrease in size observed, we designed an experiment in which DPA-ale-Endorem was prepared using heating for 15 or 30 min. The same experiments were done with Endorem without the addition of DPA-ale to test if the amount of BP used had an effect. The hydrodynamic size of each preparation was measured using DLS showing a 15 ± 5 nm decrease in all heated samples that was independent of the presence of bisphosphonate. Longer heating times resulted in particle precipitation with both samples. We therefore attribute the decrease in size to the weakening of the dextran-Fe_3O_4 interaction during heating that may result in the fragmentation of the ~120 nm core-dextran adducts. Indeed, a small population of nanoparticles with hydrodynamic size of 7 ± 5 nm was detected in the solutions of DPA-ale-Endorem after heating (Figure 2C, bottom). If heating is continued for more than 15 min, the dextran coating is no longer capable of preventing the coagulation of the iron oxide cores, which precipitate.

The stability of ^{99m}Tc-DPA-ale-SPIO and ^{99m}Tc-DPA-ale-Endorem was tested in phosphate-buffered saline (PBS) and human serum to confirm that the bisphosphonate-iron oxide binding is stable under physiological conditions for at least 48 h at 37 °C. Incubation of ^{99m}Tc-DPA-ale-SPIO in PBS showed that the BP-iron oxide bonding was very stable with

[3]The difference in size between the metal cores (5 nm, TEM) and the hydrodynamic size (120 nm, DLS) is not surprising, as Endorem in solution is formed of groups iron oxide crystals inside a larger dextran nanoparticle (Kumar, C. S. S. R. Magnetic nanomaterials; Wiley-VCH: Weinheim, 2009).

only 5% of ^{99m}Tc detaching from the iron oxide every 24 h. After 48 h, 90% of ^{99m}Tc was still bound to the SPIO particles. The radiolabeled particles were also incubated in serum and showed only a slight release of ^{99m}Tc throughout the experiment, with the presence of 15% of unbound ^{99m}Tc in the supernatant at 48 h. There was, however, substantial precipitation of the radiolabeled nanoparticles during the experiments. In the case of ^{99m}Tc-DPA-ale-Endorem (Figure S2, supporting information), the stability in human serum and PBS was higher than with ^{99m}Tc-DPA-ale-SPIO, presumably due to the protective effect of the polymeric coating. The stability in serum (96 ± 2% at 24 h and 94 ± 4% at 48 h) was also slightly lower than in PBS (100% at 48 h)). It is well known that serum proteins are adsorbed onto iron oxide materials (49, 59). We thus may attribute the minor decrease in stability observed in serum to ligand exchange mechanisms on the metal oxide surface and/or decomposition of the iron oxide particles (possibly aided by iron-binding proteins such as transferrin or ferritin). No coagulation or precipitation was observed during the experiment with ^{99m}Tc-DPA-ale-Endorem, further demonstrating its colloidal stability under physiological conditions for at least 48 h.

MRI relaxivity measurements (r_2) at 9.4 T were also performed with solutions of DPA-ale-Endorem and Endorem to investigate the effect of the labeling on the relaxometric properties. The transverse relaxation rate R_2 (s^{-1}) was calculated for samples of different concentrations of both compounds and these were plotted against iron concentration. The data points obtained were then fitted to a straight line and the slope (relaxivity r_2) calculated (Figure 3A). The r_2 value obtained for DPA-ale-Endorem was 26 s^{-1} mM^{-1} whereas for Endorem was 32 s^{-1} mM^{-1}. The decrease in r_2 observed is consistent with the decrease in hydrodynamic size found in the DLS studies (*vide supra*) and with previous reports that examined the relaxivity of fractionated Endorem (60). It must be noted, however, that the difference found in r_2 is not statistically significant ($P = 0.8$, Student's unpaired *t*-test).

Prior to the *in vivo* imaging studies, a preliminary phantom study was also prepared to validate the dual-modality imaging capabilities of ^{99m}Tc-DPA-ale-Endorem. Thus, two centrifuge tubes were loaded with a 1 mL solution of ^{99m}Tc-DPA-ale-Endorem of very low specific activity (50 kBq, 100 μg Fe). One of the tubes was centrifuged for 20 min at 17,000 g, resulting in the complete accumulation of the radiolabeled nanoparticles in a pellet at the base of the tube. The two tubes were then imaged in the 9.4 T MRI and nanoSPECT/CT scanners (Figure 3B-C). The T_2*-weighted MR image reveals the difference in the contrast of the two samples as a result of the removal of ^{99m}Tc-DPA-ale-Endorem from solution and a very strong negative signal arising from the pellet. Similarly, the nanoSPECT/CT image shows an intense SPECT signal from the pellet of ^{99m}Tc-DPA-ale-Endorem, whereas in the non-pelleted tube the SPECT signal is distributed throughout the 1 mL solution and does not appear at the image thresholds chosen. The *in vitro* experiments described above encouraged us to perform studies *in vivo*.

SPECT-CT and MR imaging studies were performed with C57BL/6 mice to confirm that ^{99m}Tc and iron oxide in ^{99m}Tc-DPA-ale-Endorem co-localize in the liver and spleen, and hence that it functions as a dual-modality SPECT-MR agent *in vivo*. T_2*-weighted MR images of the chest and abdominal area were obtained before and after intravenous injection of ^{99m}Tc-DPA-ale-Endorem and demonstrate that the agent rapidly accumulates in the liver

and spleen (~10 min after *i.v.* administration), as is usually observed for Endorem (Figure 4). Rapid uptake in the RES system with ^{99m}Tc-DPA-ale-Endorem was expected because changes in size and composition (*vide supra*) compared to its precursor are insignificant (only 3% of the surface of ^{99m}Tc-DPA-ale-Endorem is covered by ^{99m}Tc-DPA-ale or DPA-ale). Furthermore, the small size of ^{99m}Tc-DPA-ale compared to that of the dextran coating polymer units, suggest that the latter will dominate its surface properties and hence its biodistribution. The contrast in the liver was measured from the short-axis images by calculating the pre- and post-injection T_2* values using different echo times (TE) (Figure S3, Supporting information). Thus, the T_2* value of liver tissue in normal conditions was 3.3 ms, compared to a post-injection T_2* value of 1.2 ms. The shortening in the T_2* value correlates with the signal intensity decrease as a result of the strong SPIO susceptibility effects, making the organ appear darker and demonstrating high accumulation of ^{99m}Tc-DPA-ale-Endorem in the liver (Figure 4A-B).

The accumulation of ^{99m}Tc-DPA-ale-Endorem in the liver and spleen was also ascertained by whole-body nanoSPECT-CT (Figures 5A and 4C). After the MRI study the mouse was transferred to the nanoSPECT-CT scanner and an image was acquired, showing uptake of ^{99m}Tc-DPA-ale-Endorem in the liver and spleen, as seen in the MR studies. Notably, no uptake was detected in bone tissue, which is the target of ^{99m}Tc-DPA-ale when not bound to particles (Figure 5B), confirming that ^{99m}Tc-DPA-ale and Endorem co-localize and hence, the *in vivo* stability of the BP-Endorem bond (52, 61).[4] This is in agreement with expectations that the bisphosphonate group is bound to the iron oxide surface and not available for binding to bone mineral. One of the big advantages of having a radiolabeled imaging agent is the ability to quantify the amount of agent in each organ. This is difficult to do accurately with iron oxide agents using MRI (60). By using the whole-body SPECT image, we calculated that 97% of the injected dose (% ID) of ^{99m}Tc-DPA-ale-Endorem accumulated in the liver, 2% in the spleen and 1% in the rest of the body. The dual-modality nature of this agent allows us to estimate that this corresponds to an uptake of 54 μg, 2 μg and 0.5 μg of Endorem, respectively. *Ex vivo* biodistribution studies are also in agreement with the imaging studies and allow accurate quantification in each organ of the distribution of ^{99m}Tc-DPA-ale-Endorem *in vivo* (values represent the mean ± SD for 3 mice). Hence, 96.9 ± 0.9% ID was found in the liver, 1.3 ± 0.4% ID in the spleen and 1.8 ± 0.7% ID for the remaining organs. In order to compare these values with the biodistribution of non-particle-bound ^{99m}Tc-DPA-ale, the percentage of the injected dose per gram of tissue (% ID/g) was calculated (Figure 5A, right). Thus, 129 ± 27% ID/g was found in the liver and 35 ± 25% ID/g in the spleen. The remaining soft-tissue organs showed very low levels of uptake (≤3% ID/g). The uptake in bone tissue (measured as the uptake in one femur) was also negligible (2 ± 1% ID/g), in contrast to that found with ^{99m}Tc-DPA-ale (27 ± 5% ID/g) (52) and demonstrates the high *in vivo* stability of the bisphosphonate-iron oxide interaction (Figure 5B, right).

[4]As with most hydrophilic small-molecule radiotracers, the blood half-life of ^{99m}Tc-DPA-Ale is very short <5 min. Thus, one would expect to see bone uptake if ^{99m}Tc-DPA-Ale and Endorem dissociate in blood before it is taken by the RES system (~10 min). Furthermore, in vitro experiments in human serum (see text) suggest the ^{99m}Tc-DPA-Ale-Endorem remains unaltered for at least 48 h.

Conclusions

In this report we have shown that radiolabeled BP conjugates are useful compounds to label iron-oxide nanoparticles to make SPECT/PET-MR dual-modality imaging agents. We have demonstrated the concept *in vivo* with Endorem/Feridex, a clinically-approved SPIO MR imaging agent of the RES system (liver and spleen). The binding of the BP to Endorem was demonstrated by EDX studies and Dittmer-Lester TLC tests. Furthermore, labeling experiments demonstrate that the BP does not interact with dextran (the polymer coating of Endorem) and but instead binds to the Fe_3O_4 cores of Endorem. TEM studies show that the labeling process does not change the size of the Fe_3O_4 core of the nanoparticles. DLS studies, however, have shown that the hydrodynamic size of the dextran-Fe_3O_4 particles is decreased slightly (by ~6%) due to heating during labeling. The small decrease in hydrodynamic size, however, does not to affect the relaxometric properties of the particles or its MRI contrast properties significantly. The BP-Endorem binding is highly stable *in vitro* and *in vivo.* MRI, SPECT-CT imaging and biodistribution studies have demonstrated the dual-modality contrast capabilities of ^{99m}Tc-DPA-ale-Endorem by showing that it accumulates in the same organs (liver and spleen) as its precursor, Endorem, *in vivo* as expected from the lack of change in size and composition after radiolabeling. To the best of our knowledge, this is the first example of using BPs to radiolabel iron oxide nanoparticles and the first example of radiolabeling SPIOs directly onto the surface of the iron oxide core, and not its coating. Radiolabeling of iron oxide nanoparticles allows simple and accurate quantification of their biodistribution *in vivo* using SPECT or PET instrumentation, taking advantage of the higher sensitivity of these techniques compared to MRI. This work represents our first step in the development of new generations of dual-modality SPECT/PET-MR imaging agents based on bisphosphonate-iron oxide nanoparticle conjugates. We believe the BP group is a promising candidate for the simple functionalization of metal oxide nanomaterials with radionuclides, targeting molecules and stability/stealth groups for targeted radionuclide-based dual-modality medical imaging. Future work will be aimed at exploring their potential.

Supplementary Material

Refer to Web version on PubMed Central for supplementary material.

Acknowledgements

We thank Dr. Jim Ballinger and the staff at the radiopharmacy of Guys' and St. Thomas' Hospital in London for providing us with ^{99m}Tc-pertechnetate, Covidien for providing us with Isolink kits, Dr. Mark Green (Department of Physics, KCL, London) for access to the DLS instrument, Dr. Kavitha Sunassee and Istvan Szanda for assistance with the nanoSPECT-CT scanner and Dr. Rick Southworth for assistance with the MRI scanner. This work was funded by the Centre of Excellence in Medical Engineering funded by the Wellcome Trust and EPSRC under grants (WT 088641/Z/09/Z) and Cancer Research UK (C789/A7649).

Literature Cited

(1). For a dedicated recent issue of Chemical Reviews on medical imaging and diagnostics see: Chem Rev. 2010; 110(5)

(2). Baker M. Whole-animal imaging: The whole picture. Nature. 2010; 463:977–80. [PubMed: 20164931]

(3). Pichler BJ, Kolb A, Nagele T, Schlemmer H-P. PET/MRI: Paving the Way for the Next Generation of Clinical Multimodality Imaging Applications. J Nucl Med. 2010; 51:333–336. [PubMed: 20150252]

(4). Herzog H, Pietrzyk U, Shah NJ, Ziemons K. The current state, challenges and perspectives of MR-PET. NeuroImage. 2010; 49:2072–2082. [PubMed: 19853045]

(5). Wehrl HF, Judenhofer MS, Wiehr S, Pichler BJ. Pre-clinical PET/MR: technological advances and new perspectives in biomedical research. Eur J Nucl Med Mol Imaging. 2009; 36:56–68.

(6). Ha S, Hamamura MJ, Roeck WW, Muftuler LT, Nalcioglu O. Development of a new RF coil and gamma-ray radiation shielding assembly for improved MR image quality in SPECT/MRI. Phys Med Biol. 2010; 55:2495–504. [PubMed: 20371909]

(7). Catana C, Procissi D, Wu Y, Judenhofer MS, Qi J, Pichler BJ, Jacobs RE, Cherry SR. Simultaneous in vivo positron emission tomography and magnetic resonance imaging. Proc Natl Acad Sci U S A. 2008; 105:3705–10. [PubMed: 18319342]

(8). Mackewn JE, Strul D, Hallett WA, Halsted P, Page RA, Keevil SF, Williams SCR, Cherry SR, Marsden PK. Design and development of an MR-compatible PET scanner for imaging small animals. IEEE Trans Nucl Sci. 2005; 52:1376–1380.

(9). Schlemmer HPW, Pichler BJ, Schmand M, Burbar Z, Michel C, Ladebeck R, Jattke K, Townsend D, Nahmias C, Jacob PK, Heiss WD, et al. Simultaneous MR/PET imaging of the human brain: Feasibility study. Radiology. 2008; 248:1028–1035. [PubMed: 18710991]

(10). Zaidi H, Mawlawi O, Orton CG. Simultaneous PET/MR will replace PET/CT as the molecular multimodality imaging platform of choice. Med Phys. 2007; 34:1525–1528. [PubMed: 17555233]

(11). Shao YP, Cherry SR, Farahani K, Meadors K, Siegel S, Silverman RW, Marsden PK. Simultaneous PET and MR imaging. Phys Med Biol. 1997; 42:1965–1970. [PubMed: 9364592]

(12). Lucas AJ, Hawkes RC, Ansorge RE, Williams GB, Nutt RE, Clark JC, Fryer TD, Carpenter TA. Development of a combined microPET-MR system. Technol Cancer Res Treat. 2006; 5:337–41. [PubMed: 16866564]

(13). Louie A. Multimodality imaging probes: design and challenges. Chem Rev. 2010; 110:3146–95. [PubMed: 20225900]

(14). Jennings LE, Long NJ. 'Two is better than one'--probes for dual-modality molecular imaging. Chem Commun. 2009:3511–24.

(15). Lee S, Chen X. Dual-modality probes for in vivo molecular imaging. Mol Imaging. 2009; 8:87–100. [PubMed: 19397854]

(16). Kim J, Piao Y, Hyeon T. Multifunctional nanostructured materials for multimodal imaging, and simultaneous imaging and therapy. Chem Soc Rev. 2009; 38:372–90. [PubMed: 19169455]

(17). Cheon J, Lee JH. Synergistically Integrated Nanoparticles as Multimodal Probes for Nanobiotechnology. Acc Chem Res. 2008; 41:1630–1640. [PubMed: 18698851]

(18). Bligh SWA, Sadler PJ, Marriott JA, Latham IA, Kelly JD. Characterization and In vivo distribution of Tc-99m-labelled and In-111-labelled magnetite. Appl Radiat Isot. 1989; 40:751–757.

(19). Lewin M, Carlesso N, Tung CH, Tang XW, Cory D, Scadden DT, Weissleder R. Tat peptide-derivatized magnetic nanoparticles allow in vivo tracking and recovery of progenitor cells. Nat Biotechnol. 2000; 18:410–414. [PubMed: 10748521]

(20). Choi JS, Park JC, Nah H, Woo S, Oh J, Kim KM, Cheon GJ, Chang Y, Yoo J, Cheon J. A hybrid nanoparticle probe for dual-modality positron emission tomography and magnetic resonance imaging. Angew Chem Int Ed. 2008; 47:6259–62.

(21). Lee H-Y, Li Z, Chen K, Hsu AR, Xu C, Xie J, Sun S, Chen X. PET/MRI Dual-Modality Tumor Imaging Using Arginine-Glycine-Aspartic (RGD)-Conjugated Radiolabeled Iron Oxide Nanoparticles. J Nucl Med. 2008; 49:1371–1379. [PubMed: 18632815]

(22). Kaufner L, Cartier R, Wustneck R, Fitchner I, Pietschmann S, Bruhn H, Thunemann F, Pison U. Poly(ethylene oxide)- block -poly(glutamic acid) coated maghemite nanoparticles: in vitro characterization and in vivo behaviour. Nanotechnology. 2007; 18:115710.

(23). Jarrett BR, Gustafsson B, Kukis DL, Louie AY. Synthesis of ^{64}Cu-labeled magnetic nanoparticles for multimodal imaging. Bioconjugate Chem. 2008; 19:1496–504.

(24). Devaraj NK, Keliher EJ, Thurber GM, Nahrendorf M, Weissleder R. 18F labeled nanoparticles for in vivo PET-CT imaging. Bioconjugate Chem. 2009; 20:397–401.

(25). Nahrendorf M, Zhang H, Hembrador S, Panizzi P, Sosnovik DE, Aikawa E, Libby P, Swirski FK, Weissleder R. Nanoparticle PET-CT imaging of macrophages in inflammatory atherosclerosis. Circulation. 2008; 117:379–87. [PubMed: 18158358]

(26). Glaus C, Rossin R, Welch MJ, Bao G. In Vivo Evaluation of ^{64}Cu-Labeled Magnetic Nanoparticles as a Dual-Modality PET/MR Imaging Agent. Bioconjugate Chem. 2010; 21:715–722.

(27). Liu SJ, Jia B, Qiao RR, Yang Z, Yu ZL, Liu ZF, Liu K, Shi JY, Han OY, Wang F, Gao MY. A Novel Type of Dual-Modality Molecular Probe for MR and Nuclear Imaging of Tumor: Preparation, Characterization and in Vivo Application. Mol Pharm. 2009; 6:1074–1082. [PubMed: 19527074]

(28). Xie J, Chen K, Huang J, Lee S, Wang J, Gao J, Li X, Chen X. PET/NIRF/MRI triple functional iron oxide nanoparticles. Biomaterials. 2010; 31:3016–3022. [PubMed: 20092887]

(29). Bowtell R. Medical imaging: Colourful future for MRI. Nature. 2008; 453:993–994. [PubMed: 18563140]

(30). Bulte JWM, Modo MMJJ. Nanoparticles in biomedical imaging : emerging technologies and applications. Springer; New York: 2008.

(31). Jun YW, Lee JH, Cheon J. Chemical design of nanoparticle probes for highperformance magnetic resonance imaging. Angew Chem Int Ed. 2008; 47:5122–35.

(32). Na HB, Song IC, Hyeon T. Inorganic Nanoparticles for MRI Contrast Agents. Adv Mater. 2009; 21:2133–2148.

(33). Thiesen B, Jordan A. Clinical applications of magnetic nanoparticles for hyperthermia. Int J Hyperther. 2008; 24:467–474.

(34). Fortin J-P, Wilhelm C, Servais J, Ménager C, Bacri J-C, Gazeau F. Size-Sorted Anionic Iron Oxide Nanomagnets as Colloidal Mediators for Magnetic Hyperthermia. J Am Chem Soc. 2007; 129:2628–2635. [PubMed: 17266310]

(35). Kohler N, Sun C, Fichtenholtz A, Gunn J, Fang C, Zhang M. Methotrexate-immobilized poly(ethylene glycol) magnetic nanoparticles for MR imaging and drug delivery. Small. 2006; 2:785–92. [PubMed: 17193123]

(36). McCarthy JR, Weissleder R. Multifunctional magnetic nanoparticles for targeted imaging and therapy. Adv Drug Delivery Rev. 2008; 60:1241–51.

(37). Wunderbaldinger P, Josephson L, Weissleder R. Crosslinked iron oxides (CLIO): a new platform for the development of targeted MR contrast agents. Acad Radiol. 2002; 9(Suppl 2):S304–6. [PubMed: 12188255]

(38). Fleisch H. Bisphosphonates: mechanisms of action. Endocrine Rev. 1998; 19:80–100. [PubMed: 9494781]

(39). Portet D, Denizot B, Rump E, Lejeune JJ, Jallet P. Nonpolymeric Coatings of Iron Oxide Colloids for Biological Use as Magnetic Resonance Imaging Contrast Agents. J Colloid Interface Sci. 2001; 238:37–42. [PubMed: 11350133]

(40). Gao W, Dickinson L, Grozinger C, Morin FG, Reven L. Self-Assembled Monolayers of Alkylphosphonic Acids on Metal Oxides. Langmuir. 1996; 12:6429–6435.

(41). Rutledge RD, Warner CL, Pittman JW, Addleman RS, Engelhard M, Chouyyok W, Warner MG. Thiol–Ene Induced Diphosphonic Acid Functionalization of Superparamagnetic Iron Oxide Nanoparticles. Langmuir. 2010; 26:12285–12292. [PubMed: 20550201]

(42). Sahoo Y, Pizem H, Fried T, Golodnitsky D, Burstein L, Sukenik CN, Markovich G. Alkyl Phosphonate/Phosphate Coating on Magnetite Nanoparticles: A Comparison with Fatty Acids. Langmuir. 2001; 17:7907–7911.

(43). Mohapatra S, Pramanik P. Synthesis and stability of functionalized iron oxide nanoparticles using organophosphorus coupling agents. Colloids Surf A. 2009; 339:35–42.

(44). Lalatonne Y, Paris C, Serfaty JM, Weinmann P, Lecouvey M, Motte L. Bis-phosphonates-ultra small superparamagnetic iron oxide nanoparticles: a platform towards diagnosis and therapy. Chem Commun. 2008:2553–5.

(45). Benyettou F, Lalatonne Y, Sainte-Catherine O, Monteil M, Motte L. Superparamagnetic nanovector with anti-cancer properties: gamma Fe_2O_3@Zoledronate. Int J Pharm. 2009; 379:324–7. [PubMed: 19457625]

(46). Clearfield A. Recent advances in metal phosphonate chemistry II. Curr Opin Solid State Mater Sci. 2002; 6:495–506.

(47). Amstad E, Gillich T, Bilecka I, Textor M, Reimhult E. Ultrastable iron oxide nanoparticle colloidal suspensions using dispersants with catechol-derived anchor groups. Nano Lett. 2009; 9:4042–8. [PubMed: 19835370]

(48). Amstad E, Zurcher S, Mashaghi A, Wong JY, Textor M, Reimhult E. Surface Functionalization of Single Superparamagnetic Iron Oxide Nanoparticles for Targeted Magnetic Resonance Imaging. Small. 2009; 5:1334–1342. [PubMed: 19242944]

(49). Tromsdorf UI, Bruns OT, Salmen SC, Beisiegel U, Weller H. A Highly Effective, Nontoxic T1 MR Contrast Agent Based on Ultrasmall PEGylated Iron Oxide Nanoparticles. Nano Lett. 2009; 9:4434–4440. [PubMed: 19799448]

(50). Das M, Mishra D, Dhak P, Gupta S, Maiti TK, Basak A, Pramanik P. Biofunctionalized, phosphonate-grafted, ultrasmall iron oxide nanoparticles for combined targeted cancer therapy and multimodal imaging. Small. 2009; 5:2883–93. [PubMed: 19856326]

(51). Shultz MD, Reveles JU, Khanna SN, Carpenter EE. Reactive nature of dopamine as a surface functionalization agent in iron oxide nanoparticles. J Am Chem Soc. 2007; 129:2482–7. [PubMed: 17290990]

(52). Torres Martin de Rosales R, Finucane C, Mather SJ, Blower PJ. Bifunctional bisphosphonate complexes for the diagnosis and therapy of bone metastases. Chem Commun. 2009:4847–9.

(53). Dittmer JC, Lester RL. A simple, specific spray for the detection of phospholipids on thin-layer chromatograms. J Lipid Res. 1964; 5:126–127. [PubMed: 14173318]

(54). Alberto R, Ortner K, Wheatley N, Schibli R, Schubiger AP. Synthesis and properties of boranocarbonate: a convenient in situ CO source for the aqueous preparation of $[^{99m}Tc(OH_2)_3(CO)_3]^+$ J Am Chem Soc. 2001; 123:3135–6. [PubMed: 11457025]

(55). Kang YS, Risbud S, Rabolt JF, Stroeve P. Synthesis and Characterization of Nanometer-Size Fe_3O_4 and γ-Fe_2O_3 Particles. Chem Mater. 1996; 8:2209–2211.

(56). Nancollas GH, Tang R, Phipps RJ, Henneman Z, Gulde S, Wu W, Mangood A, Russell RG, Ebetino FH. Novel insights into actions of bisphosphonates on bone: differences in interactions with hydroxyapatite. Bone. 2006; 38:617–27. [PubMed: 16046206]

(57). Jung CW. Surface-Properties of Superparamagnetic Iron-Oxide Mr Contrast Agents - Ferumoxides, Ferumoxtran, Ferumoxsil. Magn Reson Imaging. 1995; 13:675–691. [PubMed: 8569442]

(58). Sivchik VV, Zhbankov RG, Astreiko MV. Theoretical investigation of the vibrational spectrum of dextran. Acta Polym. 1979; 30:689–693.

(59). Lind K, Kresse M, Müller RH. Comparison of protein adsorption patterns onto differently charged hydrophilic superparamagnetic iron oxide particles obtained in vitro and ex vivo. Electrophoresis. 2001; 22:3514–3521. [PubMed: 11669535]

(60). Briley-Saebo KC, Mani V, Hyafil F, Cornily JC, Fayad ZA. Fractionated Feridex and positive contrast: In vivo MR imaging of atherosclerosis. Magn Reson Med. 2008; 59:721–730. [PubMed: 18383304]

(61). Torres Martin de Rosales R, Finucane C, Foster J, Mather SJ, Blower PJ. $^{188}Re(CO)_3$-dipicolylamine-alendronate: a new bisphosphonate conjugate for the radiotherapy of bone metastases. Bioconjugate Chem. 2010; 21:811–5.

Europe PMC Funders Author Manuscripts

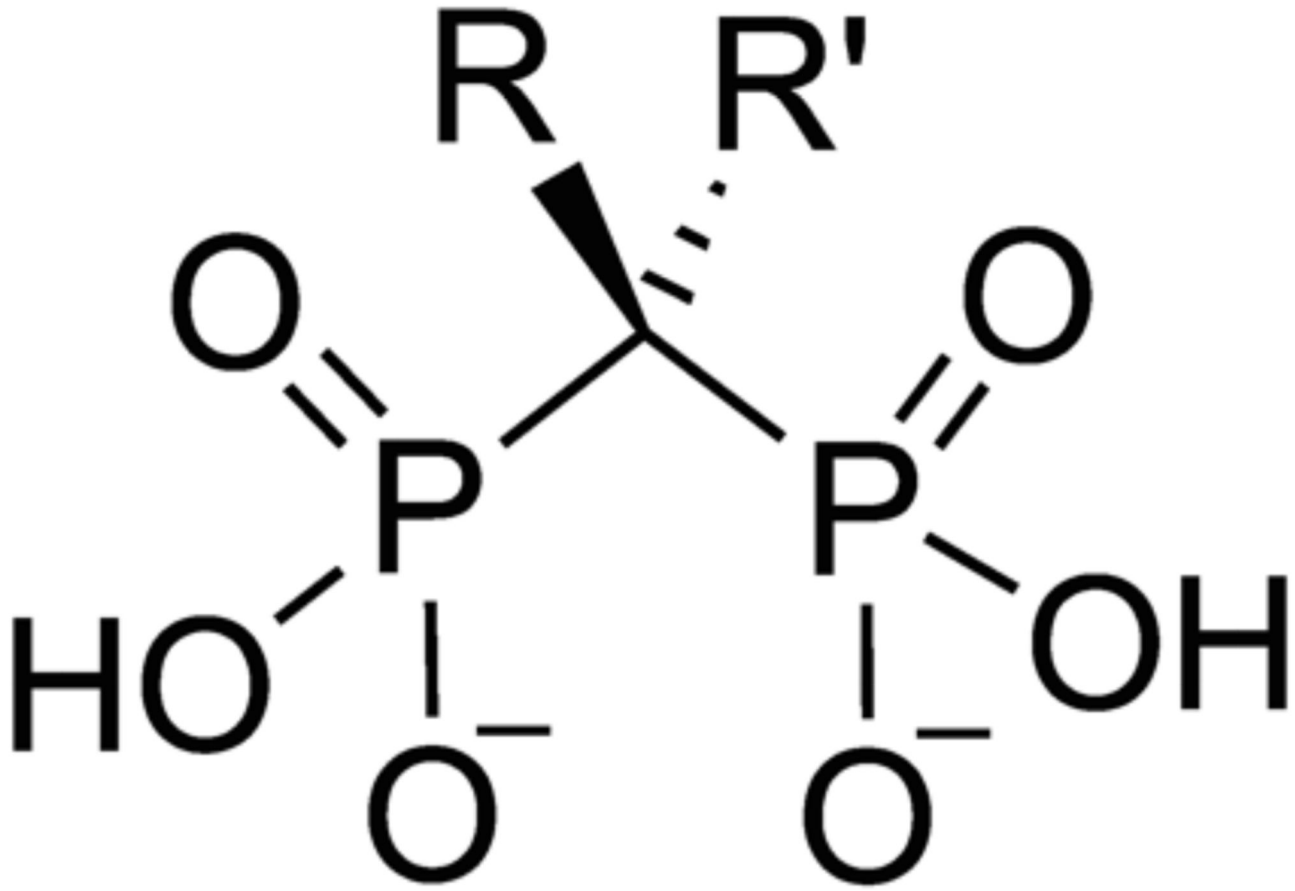

Figure 1.
General structure of a bisphosphonate (BP).

Europe PMC Funders Author Manuscripts

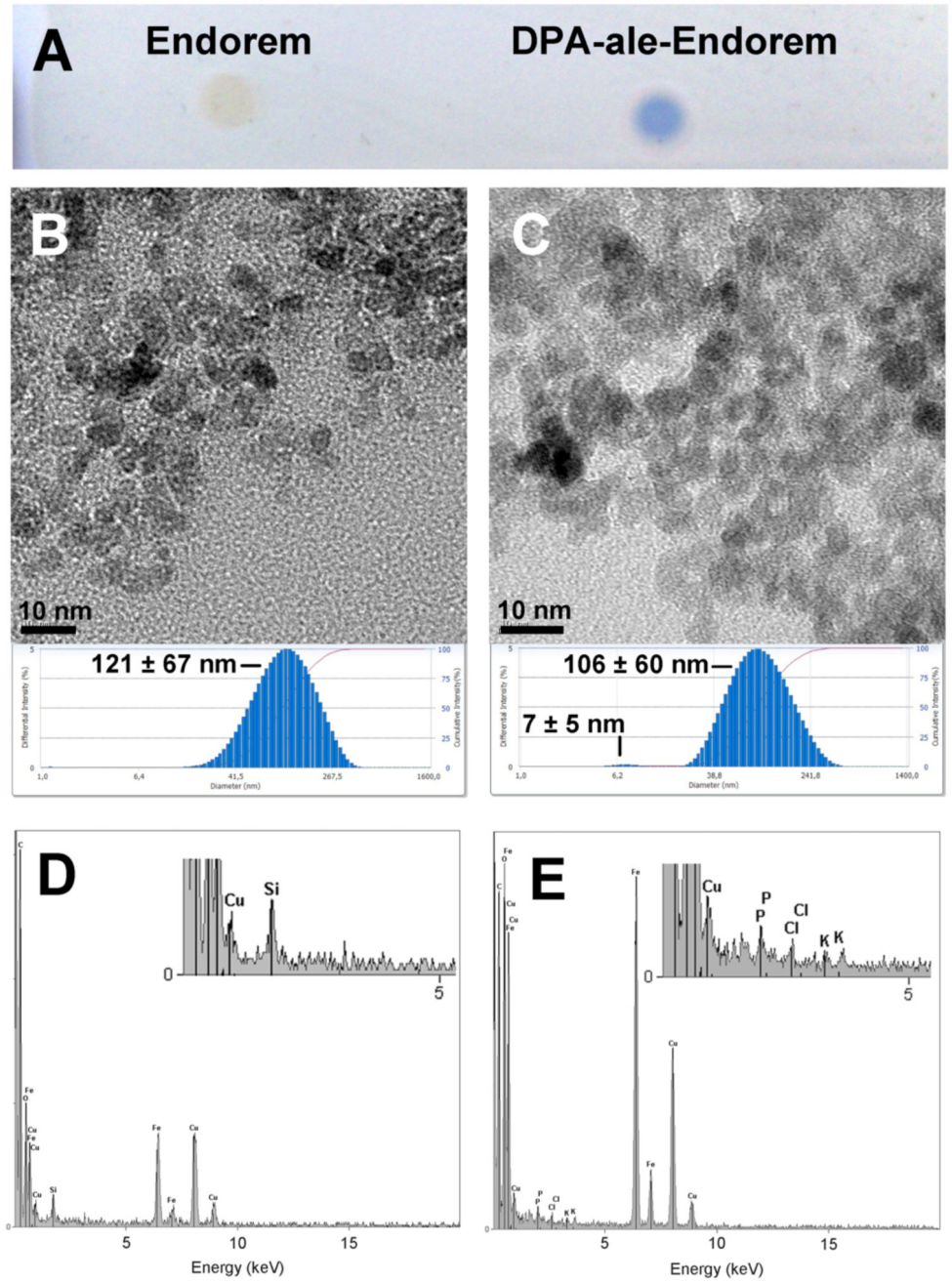

Figure 2.

BP (DPA-ale) binding to iron oxide nanoparticles (Endorem): (A) Silica TLC spots of Endorem (left) and DPA-ale-Endorem (right) after Dittmer's staining. Blue color demonstrates presence of phosphorus; (B, C) TEM pictures (top) and DLS studies (bottom) of Endorem (B) and DPA-ale-Endorem (C). (D, E) EDX studies of Endorem (D) and DPA-ale-Endorem (E). The inset is a magnification of the range between 0-5 keV. Note the presence of phosphorus in (E). A peak due to the presence of silicon is seen in (D) and is most likely to be due to contamination of the sample with vacuum grease.

Europe PMC Funders Author Manuscripts

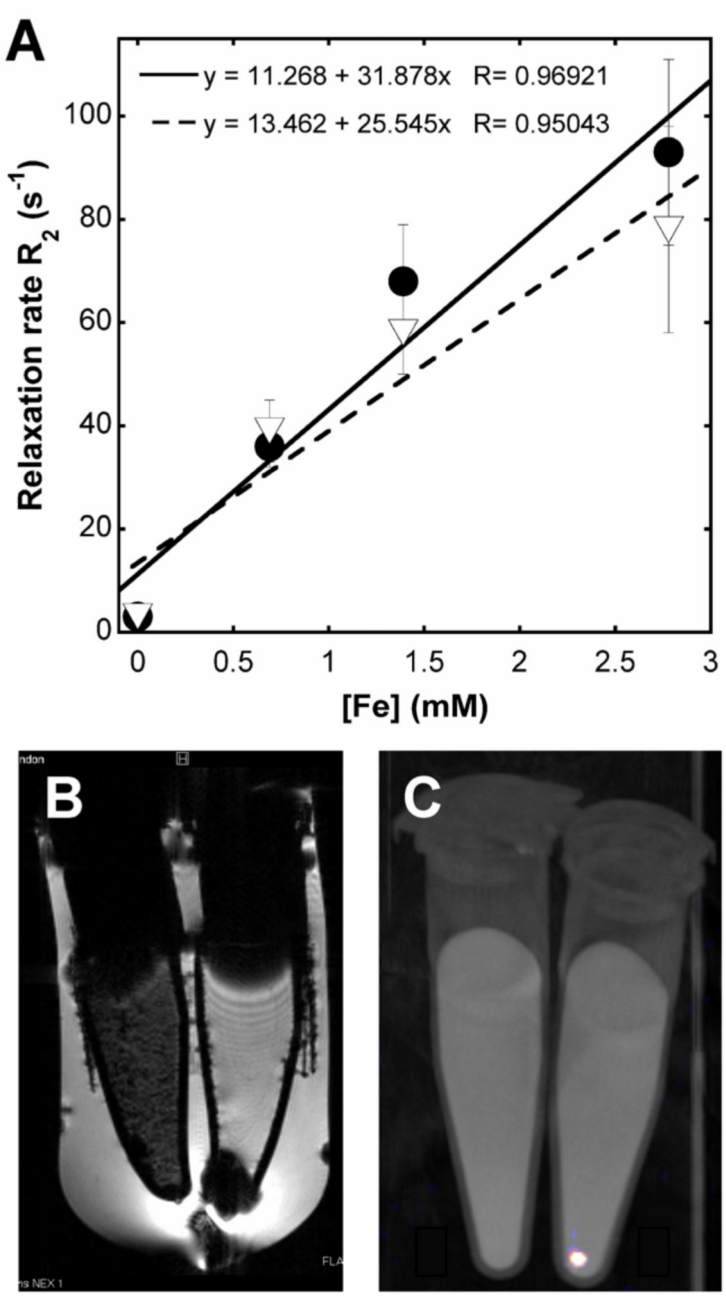

Figure 3.

In vitro imaging studies. (A) MRI relaxivity measurements of Endorem (closed circles, continuous line) and DPA-ale-Endorem (open triangles, discontinuous line) at 9.4 T. The slope of the linear fit represents the relaxivity of each sample (r_2). (B) T_2*-weighted MR phantom study of two samples containing the same amount of ^{99m}Tc-DPA-ale-Endorem. In the left tube the nanoparticles were in solution, whereas in the right tube the particles had been pelleted by centrifuging. There is a strong negative signal from the pellet in the right tube. (C) NanoSPECT-CT image of the same sample from (B). There is a strong focal

SPECT signal in the right sample, where ^{99m}Tc-DPA-ale-Endorem had concentrated, whereas the signal in the left tube is diffuse.

Europe PMC Funders Author Manuscripts

Europe PMC Funders Author Manuscripts

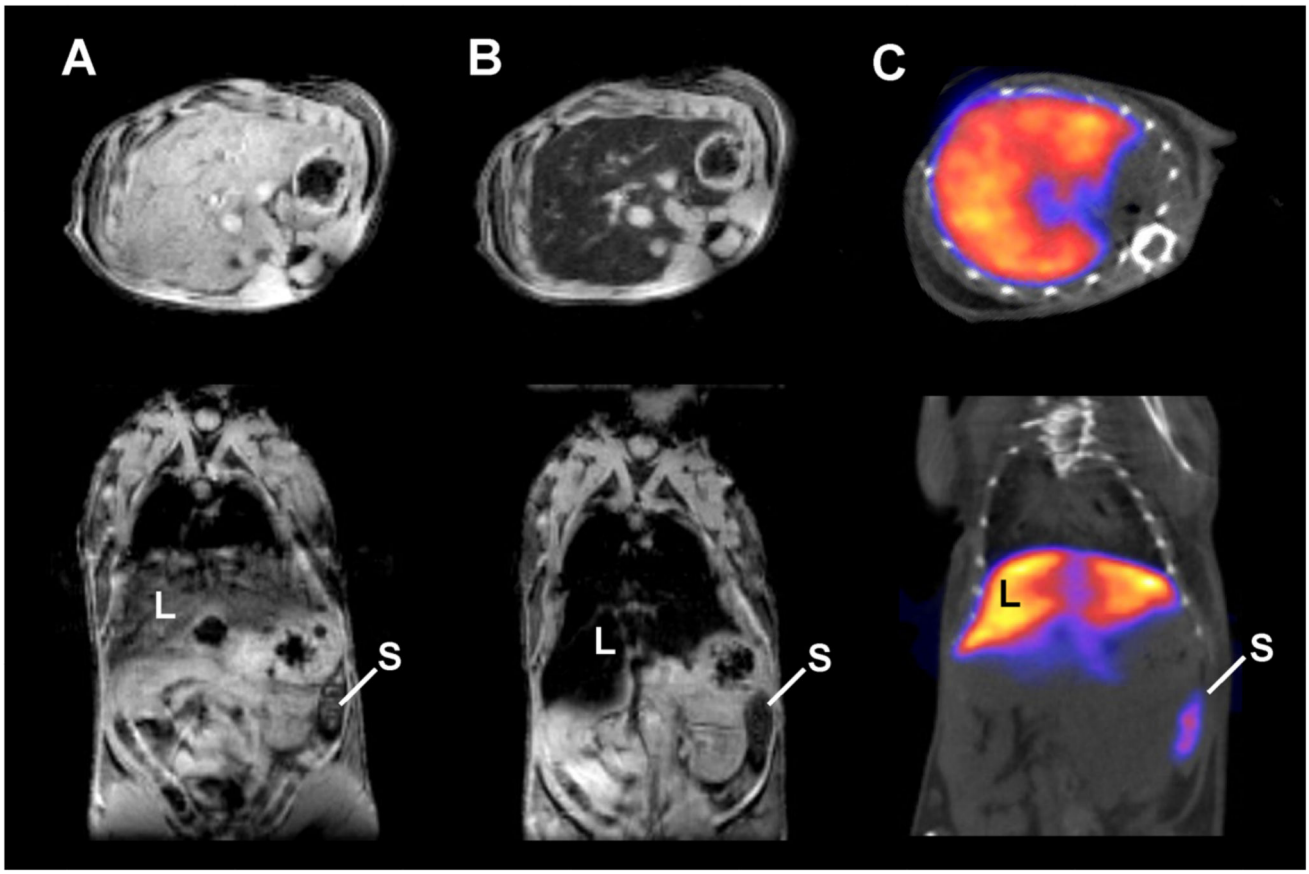

Figure 4.

Dual-modality *in vivo* studies. Short-axis view (top) and coronal view (bottom) images: (A) T_2*-weighted MR images before injection of ^{99m}Tc-DPA-ale-Endorem, (B) T_2*-weighted MR image 15 min post-injection and (C) nanoSPECT-CT image of the same animal in a similar view 45 min post-injection. Contrast in the liver (L) and spleen (S) changes after injection due to accumulation of ^{99m}Tc-DPA-ale-Endorem, in agreement with the nanoSPECT-CT image which shows almost exclusively liver and spleen accumulation of radioactivity. MR images were acquired with a TE of 2 ms.

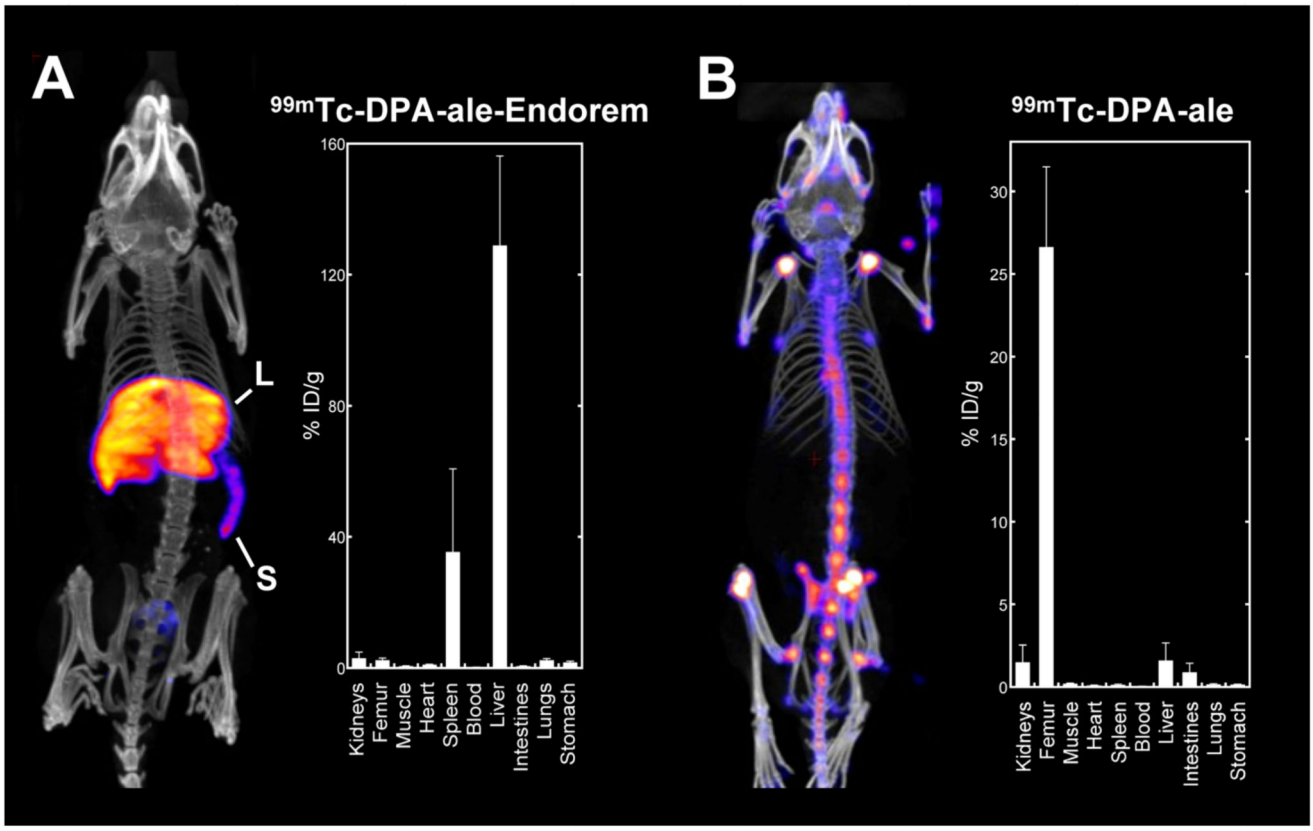

Figure 5.

In vivo studies. Whole body SPECT-CT maximum intensity projection (left) and biodistribution studies (right) of ^{99m}Tc-DPA-ale-Endorem (A) and ^{99m}Tc-DPA-ale (B). Biodistribution values represent the mean ± SD of the % ID/g (n = 3 mice).

Europe PMC Funders Author Manuscripts

Europe PMC Funders Author Manuscripts

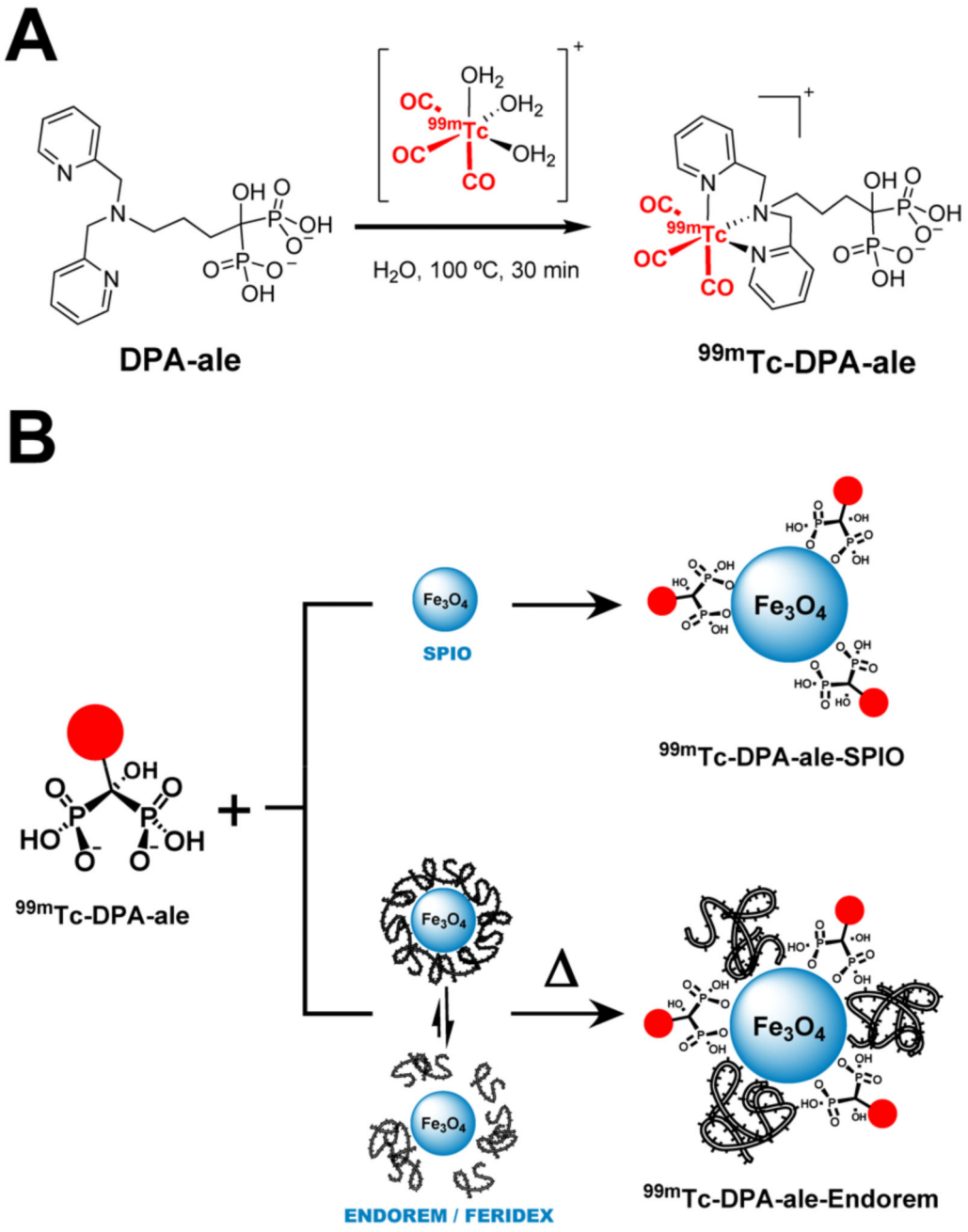

Scheme 1.

(A) Synthesis of ^{99m}Tc-DPA-ale and (B) schematic representation of the synthesis of radiolabeled SPIO nanoparticles ^{99m}Tc-DPA-ale-SPIO (top) and ^{99m}Tc-DPA-ale-Endorem (bottom).